Science of the Total Environment 818 (2022) 151698

Contents lists available at ScienceDirect

Science of the Total Environment

journal homepage: www.elsevier.com/locate/scitotenv

Vertical distribution and transport of radiocesium via branchflow and stemflow through the canopy of cedar and oak stands in the aftermath of the Fukushima Dai-ichi Nuclear Power Plant accident

Zul Hilmi Saidin [a], Delphis F. Levia [b,c], Hiroaki Kato [a], Momo Kurihara [a], Janice E. Hudson [a], Kazuki Nanko [d], Yuichi Onda [a,*]

[a] Center for Research in Isotopes and Environmental Dynamics, University of Tsukuba, Tsukuba, Ibaraki, Japan
[b] Department of Geography and Spatial Sciences, University of Delaware, Newark, DE, USA
[c] Department of Plant and Soil Sciences, University of Delaware, Newark, DE, USA
[d] Department of Disaster Prevention, Meteorology and Hydrology, Forestry and Forest Products Research Institute, Tsukuba, Ibaraki, Japan

HIGHLIGHTS

- Vertical variation of ^{137}Cs cycling was observed for both cedar and oak stands.
- 71% and 48% of the ^{137}Cs flux originated from cedar/oak upper canopies, respectively.
- ^{137}Cs concentrations in branchflow and stemflow were largest during winter.
- The annual ^{137}Cs flux from the oak stand was 7.5 times greater than cedar.

GRAPHICAL ABSTRACT

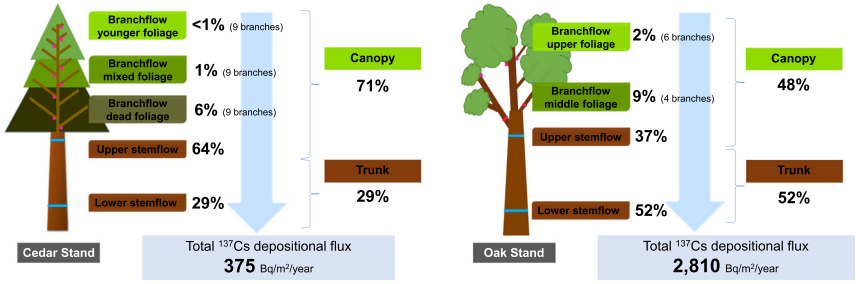

ARTICLE INFO

Article history:
Received 27 June 2021
Received in revised form 11 November 2021
Accepted 11 November 2021
Available online 16 November 2021

Editor: Manuel Esteban Lucas-Borja

Keywords:
Radiocesium contamination
Radiocesium deposition
Japanese cedar tree
Japanese oak tree

ABSTRACT

Aiming to fill a need for data regarding radiocesium transport via both branchflow and stemflow through forests impacted by radioactive fallout, this study examined the vertical variation of radiocesium flux from branchflow and stemflow through the canopies of young Japanese cedar (*Cryptomeria japonica* (L. f.) D. Don) and Japanese oak (*Quercus serrata* Murray) trees in the aftermath of the Fukushima Dai-ichi Nuclear Power Plant accident. In forested areas approximately 40 km northwest of the location of the Fukushima Dai-ichi accident, the ^{137}Cs concentration varied significantly among sampling periods and between the two forests, with the oak stand exhibiting higher ^{137}Cs concentrations and depositional fluxes than the cedar stand. Expressed per unit trunk basal area, the depositional flux of ^{137}Cs generated from the cedar and oak stands was 375 and 2810 Bq m^{-2} year^{-1}, respectively. Of this total, 71% and 48% originated from the cedar and oak canopy, respectively, while the remainder originated from the trunk. Accordingly, the origin of radiocesium was more balanced for the oak stand with almost half of the flux coming from the canopy (48%) and the other half from the trunk (52%). Only about a quarter (29%) of the radiocesium flux originated from the trunk in Japanese cedar. Results from this work provide needed data that can enable a more thorough conceptualization of radiocesium cycling in forests. Coupling these empirical results with a physically-based model would likely lead to better forest management and proactive strategies for rehabilitating radioactively-contaminated forests and reducing the exposure risk of radiation dose rate for those that utilize forest products.

* Corresponding author at: Center for Research in Isotopes and Environmental Dynamics, University of Tsukuba, Tsukuba, Ibaraki, Japan.
E-mail address: onda@geoenv.tsukuba.ac.jp (Y. Onda).

https://doi.org/10.1016/j.scitotenv.2021.151698
0048-9697/

1. Introduction

The Great East Japan Earthquake (9.0 magnitude) and subsequent tsunami on March 11, 2011 resulted in collateral damage to the nuclear reactors of the Fukushima Daiichi Nuclear Power Plant (FDNPP). This damage led to an excessive release of radionuclides, mainly as radiocesium ^{134}Cs (half-life = 2.06 years) and ^{137}Cs (half-life = 30.2 years), being unevenly dispersed onto the surrounding terrestrial ecosystem (Chino et al., 2011; MEXT, 2011a; Hirose, 2012; Onda et al., 2020). Deposition of radiocesium, and other radionuclides, decreased with increasing distance from the FDNPP, partly depending on wind direction in the days soon after the accident. The plume of radionuclides was transported by a southeasterly wind and deposited in adjacent areas toward the northwestern region (Morino et al., 2013; Tsuruta et al., 2014), predominantly within Fukushima Prefecture as dry and wet deposition. Dry deposition on March 12 carried radiocesium-containing particulate matter, aerosols, and gases to the ground surface (Kaneyasu et al., 2012; Adachi et al., 2013; Endo et al., 2015). Wet deposition followed during rain and snow events on March 15 and 16, carrying most of the remaining aerosols and water-soluble gases to the surface. The largest on-land deposition occurred on March 15 in Fukushima Prefecture when the peak radionuclide plume and dust, including radiocesium (^{134}Cs, ^{136}Cs, and ^{137}Cs), was washed out by the rainfall and/or snowfall (Chino et al., 2011; Kinoshita et al., 2011, MEXT, 2011a, 2011b; Terada et al., 2012; Morino et al., 2013). Consequently, 98% of the ^{137}Cs deposition on the land was dominated by wet deposition (Morino et al., 2013).

A large percentage of atmospheric radiocesium was deposited onto surrounding forests (Koizumi et al., 2013; Kato et al., 2019a; Onda et al., 2020) where the evergreen cedar canopy intercepted approximately 70% of the total radiocesium deposition, and deciduous broadleaved forest intercepted approximately 20% (Kato et al., 2017). Incident precipitation on these canopies can enhance the vertical migration of radiocesium via throughfall and stemflow. The existence of radiocesium, particularly ^{137}Cs substances with a long half-life is a threat to the forest ecosystem. For example, in the aftermath of Chernobyl Nuclear Power Plant (CNPP) accident, high levels of chronic radiation exposure were found to damage trees, whereby bioaccumulation through various plant tissues resulted in morphological and physiological abnormalities in some Scots pine trees (*Pinus silvestris* L.) (Geras'kin et al., 2019). Today, these damaged woodlands are being referred to as the "red forest" (IAEA, 2006). Therefore, knowing the sources of enriched radiocesium and its leaching distribution within the tree stand via throughfall or stemflow could provide insight into the behavior and fate of radiocesium that is cycled within the cedar and oak forests. Such knowledge of radiocesium cycling may be of use for ongoing decontamination efforts in an attempt to reduce dose rate exposure within the forest to safe levels.

Stemflow is a localized input of intercepted precipitation near the tree trunk and its infiltration into the surrounding soil is an important component of biogeochemical processes in the forest ecosystem (Levia and Herwitz, 2000; Levia and Frost, 2003; Imamura et al., 2017b; Kato, 2020). Intercepted rain converges onto the tree trunk from the canopy through stemflow funneling of branchflow, thereby concentrating water inputs (Carlyle-Moses et al., 2018), which can lead to groundwater recharge (Tanaka et al., 1996; Taniguchi et al., 1996). As such, stemflow is one of the radiocesium deposition pathways in addition to litterfall and throughfall. In early 2011 to 2012, the range of contribution of radiocesium deposition via stemflow was 0.6% to 2.3% compared to litterfall (39.5% to 68.5%) and throughfall (30.9% to 59.4%) in a Japanese cedar forest (Endo et al., 2015; Kato et al., 2017). For a mixed broadleaved forest, stemflow deposition was 2.6% to 6.9% compared to litterfall (43.9% to 64.0%) and throughfall (31.3% to 49.2%) (Endo et al., 2015; Kato et al., 2017). Koizumi et al. (2013) found that ^{137}Cs substances were retained and released within the biomass of the forest canopy. Thus, deposited radionuclides may be transported through branchflow and stemflow, eventually migrating to the tree trunk and subsequently concentrate in the forest floor. In fact, stemflow-induced spatial redistribution of radiocesium in the proximal areas surrounding tree trunks has been found to contribute to the circumferential variation of radiocesium stocks around konara oak trees (Imamura et al., 2017b). Therefore, despite being a lower percentage of incident precipitation than throughfall, stemflow is important to the spatial heterogeneity of radiocesium concentrations and stocks in forests.

The sourcing of radiocesium leaching via stemflow, however, is complicated by immobilization-translocation and adsorption-absorption processes, such as foliar uptake from dissolved ^{137}Cs presumably absorbed from leaf surfaces, internal translocation from older to younger foliage (Nishikiori et al., 2015; Hara et al., 2020), and adsorption and leaching between outer bark and stemflow (Sasaki et al., 2016). The disentangling of radiocesium sources between the upper canopy and lower trunk compartments and corresponding flux merits further investigation. Since stemflow has a double funneling effect both above- and belowground (Guo et al., 2020), it is important to track the transport of radiocesium vertically through the canopy and into the soils. Furthermore, knowledge of vertical variation of radiocesium stocks within the canopy are important to pinpoint radiocesium hotspots in the canopy. So, even though the stemflow flux is unified as it enters the soil, knowledge of vertical variation supplies additional information on Cs stores within the canopy and this is important for biogeochemical cycling of radiocesium. In Canada, the verticality of stemflow production was investigated for another coniferous species, whereby the upper portion of the canopy was found to generate a disproportionately high amount of the stemflow (Hutchinson and Roberts, 1981). In addition, Kuraji et al. (2001) found a variation in the ion concentration that leached from upper and lower parts of individual trees. Utilizing methods of Kuraji et al. (2001), it is possible to partition stemflow vertically to quantify radiocesium flux for different tree heights.

Previous studies elsewhere have also investigated radiocesium leaching via stemflow. In the case of the CNPP accident, stemflow research focused on dissolved forms of ^{137}Cs leachate from beech trees (Schimmack et al., 1993) and non-uniform ^{137}Cs distribution with soil depth and proximity from the trunks of the beech trees due to stemflow (Forster and Schimmack, 1992). In the case of the FDNPP accident, the research on stemflow concentrated on the fate and contribution of radiocesium leaching via stemflow, from initial deposition onto the canopy to deposition on forest floor (Loffredo et al., 2014; Teramage et al., 2014; Endo et al., 2015; Niizato et al., 2015; Kato et al., 2017), rather than the vertical variation of stemflow flux. As expected, higher amounts of ^{137}Cs were found in stemflow shortly after the accident and decreased with time (Kato et al., 2019b; Onda et al., 2020). Larger ^{137}Cs concentrations and stocks were found in the proximal areas of tree trunks (as opposed to distal areas) of oak stands with the circumferential variation of stemflow inputs around trees explaining spatial patterns in near-trunk soils (Imamura et al., 2017b).

Despite progress in radiocesium measurement and monitoring in forest ecosystems, few studies have focused solely on stemflow. Therefore, with a focus on stemflow and branchflow, this study aimed to clarify the vertical variability of radiocesium distribution and transport in a coniferous forest (*Cryptomeria japonica* (L. f.) D. Don, Japanese cedar) and a mixed deciduous broadleaved forest (*Quercus serrata* Murray, Japanese oak). This study builds upon earlier work that has investigated radiocesium deposition onto forest canopies and the subsequent cycling via throughfall and stemflow (as reviewed above) and delves into the vertical variation of radiocesium cycling within the forest canopy. Such an objective is novel since it is the first known study to examine both branchflow and stemflow cycling of radiocesium and how it is altered by both canopy height and by season. Thus, results from this work will provide needed data that will enable a more thorough conceptualization of radiocesium cycling in forests. Once a better

understanding of radiocesium cycling is achieved, forest managers will be able to develop proactive strategies to rehabilitate forests and reduce risk for those that utilize forest products.

2. Material and methods

2.1. Study site description

The study sites were located approximately 40 km northwest of the FDNPP, in Yamakiya District, Kawamata Town, Fukushima Prefecture. Two experimental plots were selected in different forest stands: a coniferous forest (37°35′08.8″ N, 140°41′26.1″ E, 556 m above sea level) and a mixed deciduous broadleaved forest (37°36′09.2″ N, 140°40′37.8″ E, 580 m above sea level) (Fig. 1). The distance between these forest stands was approximately 2 km. The coniferous forest was a plantation forest dominated by young Japanese cedar stands. The deciduous mixed broadleaved forest was a secondary forest where four Japanese oak, two Japanese red pine (*Pinus densiflora* Sieb. et Zucc.) and one forked viburnum (*Viburnum furcatum* Blume ex Maxim.) grew within the plots (Kato et al., 2019b).

These plots have been intensively monitored for radiocesium deposition from June 2011 via prior studies, which examined the hydrological partitioning and temporal changes in radiocesium activity at earlier and later stages (Coppin et al., 2016; Kato et al., 2017; Kato et al., 2019b; Onda et al., 2020), radiocesium in the soil profile and litter layer (Takahashi et al., 2015; Kurihara et al., 2018; Takahashi et al., 2019) and modeling of canopy radiocesium leaching (Loffredo et al., 2014, 2015). Briefly, the plot of Japanese cedar had a mean dbh of 18.7 cm, a stand density of 2600 trees ha^{-1}, a stand basal area of 68.4 m^2 ha^{-1} and mean tree height of 11 m, while the deciduous mixed broadleaved plot had a mean dbh of 12.0 cm, a stand density of 2500 trees ha^{-1}, a stand basal area of 19.2 m^2 ha^{-1} and mean tree height of 25 m. Readers are referred to Kato et al. (2019b) for a more detailed description of the plots.

The amount of initial fallout of radioactive materials is relatively high in the Kawamata area (where the study plots were located). The total deposition density of radiocesium (^{134}Cs and ^{137}Cs) was estimated in the range of 0.3–3.0 MBq m^{-2}. The total ^{137}Cs deposition as measured during the 3rd airborne monitoring survey conducted in July 2011 among the young cedar stand and mixed broadleaved stand were 442 ± 30 kBq m^{-2} and 451 ± 17 kBq m^{-2}, respectively (MEXT, 2011a). Cumulative ^{137}Cs deposition (via stemflow, throughfall and litterfall over the whole monitoring period) from 2011 to 2012 within these plots onto the young cedar and broadleaved deciduous stands were 105 kBq m^{-2} and 42 kBq m^{-2}, respectively (Kato et al., 2017). The mean and median of ^{137}Cs deposition density in the Kawamata forested area were 292 kBq m^{-2} and 223 kBq m^{-2}, respectively, with the ^{137}Cs inventory in the forested area being 27 TBq (Kato and Onda, 2018). These values are based on the 3rd and 5th airborne surveys conducted by MEXT with the corrected variation and reduced uncertainties from the initial fallout.

Air temperature was recorded at Nihonmatsu weather station (37°35.0′ N, 140°2′ E) by Japan Meteorological Agency and precipitation was recorded at Yamakiya weather station (37°36′ N, 140°40′ E) by the Water Information System of Ministry of Land, Infrastructure, Transport and Tourism, Japan. The mean annual total precipitation and mean annual air temperature and their standard deviations from 2000 to 2018 in this area were 1240 ± 185 mm and 12.3 °C ± 0.43, respectively. High seasonal variation in precipitation was observed at the study sites. Two dominant rainy seasons (summer monsoon rainy season and autumn rainy season), from July to October account for 57% of the mean annual total of precipitation, while during the winter period from December to February, rain or snowfall can occur. The predominant wind direction for 2018 was from the west and maximum wind speed was 14.0 m s^{-1}, recorded at the Nihonmatsu weather station. The mean wind speed inside the forest was 0.015 m s^{-1} (Kato et al., 2013).

2.2. Hydrological measurements over the study period

Branchflow and stemflow were monitored from October 2017 to December 2018 in the cedar forest and from February 2018 to December 2018 in the mixed broadleaved deciduous forest. In total, over the course of the study, there were 91 rain days in the oak stand and 118 rain days in the cedar stand, corresponding well to the annual average of 112 rain days per year in parts of Fukushima Prefecture. The collection of branchflow and stemflow occurred after the rain event and the cessation of branchflow and stemflow. For the assessment of seasonal

Fig. 1. Location of the study sites. The total radiocesium deposition density map is based on airborne monitoring on November 18, 2016 by MEXT (2011a). Retrieved from http://ramap.jmc.or.jp/map/eng/ on August 4, 2017.

patterns, sampling periods in the cedar and oak stands were categorized into four seasons (Table S1 in supplementary data). The seasons were defined as following: spring (March–May), summer (June–August), autumn (September–November) and winter (December–February).

2.3. Branchflow and stemflow sampling

Three cedar trees (Cedar A, Cedar B and Cedar C) and two oak trees (Oak 1 and Oak 3) were selected for stemflow monitoring. The basal areas of the cedar trees were 0.286 m^2 (Cedar A), 0.196 m^2 (Cedar B) and 0.281 m^2 (Cedar C), respectively, while the basal areas of the oak trees were 0.575 m^2 (Oak 1) and 0.624 m^2 (Oak 3), respectively. The position of installed branchflow and stemflow collectors within the tree stands of cedar and oak are described in Fig. 2a and b, respectively. To best account for vertical variation of branchflow and stemflow over the entire height of the forest canopy, the vertical layers of the canopy where branchflow and/or stemflow were collected (see Fig. 2a–b) were divided as follows (from top to bottom): (1) for cedar, branchflow from branches with younger foliage, branchflow from branches with mixed foliage, branchflow from branches with dead foliage, upper-tree stemflow at 1 m below the last of branches with dead foliage, and lower-tree stemflow at 1.37 m from forest floor (Fig. 2a); and (2) for oak, branchflow from branches with the upper most foliage, branchflow from branches with mid-level foliage, upper-tree stemflow at 1 m

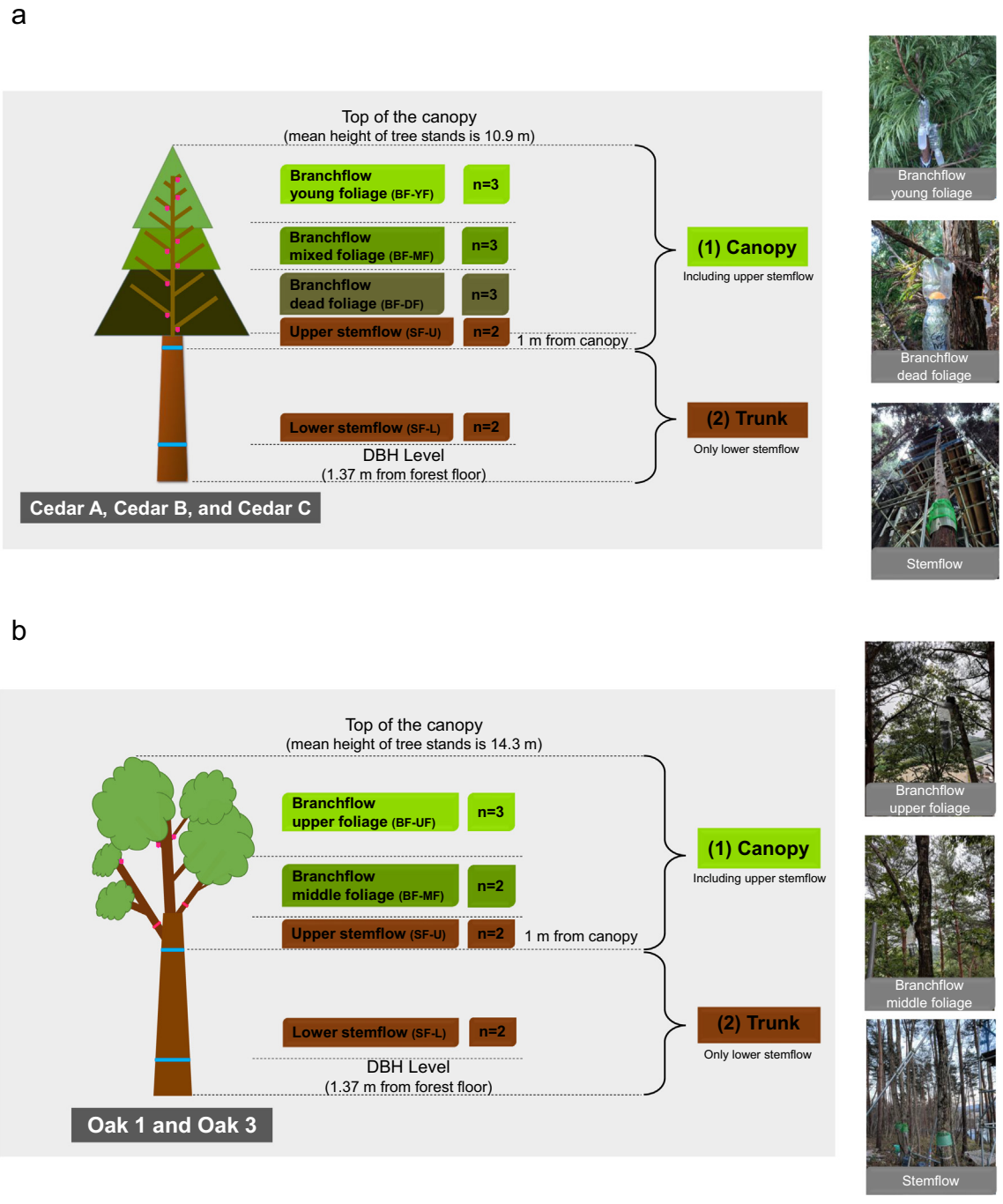

Fig. 2. a. Position and number (n) of branchflow and stemflow collectors per tree within the cedar stands. The collectors were installed in different stand compartments for Cedar A, Cedar B and Cedar C. The canopy was represented by branchflow of younger foliage, mixed foliage, dead foliage and upper stemflow. The trunk was represented by lower stemflow.
b. Position and number (n) of branchflow and stemflow collectors per tree within the oak stands. The collectors were installed in different stand compartments for Oak 1 and Oak 3. The canopy was represented by branchflow of upper foliage, middle foliage and upper stemflow. The trunk was represented by lower stemflow.

below the last branch, and stemflow at 1.37 m from forest floor for the oak stand (Fig. 2b). Branchflow collectors, installed at the base of sampled branches, were constructed from modified PET bottles (1 L capacity) and a subsample funneled to 300 mL PP bottles that were changed after each event (Fig. 2a–b). The PET and PP bottles used to collect branchflow did not overflow during the sampled events. Stemflow was collected via vinyl collars attached to the tree boles at the predescribed heights that were connected via tubing to 20 L containers on the ground. After each collection, the funnels and containers were wiped with ethanol-based wet tissues and washed with distilled water. Branchflow and stemflow were collected and their respective volumes determined for each of the different tree heights via a canopy tower installed *in situ*.

It is important to note that the branchflow collected will include water that was in contact with foliar surfaces only, branch surfaces only, or a mixture of both, just as that which occurs in nature. The same applies to stemflow on a given vertical section of the tree where branchflow converges and the water collected on that stem section could be a mixture of flow from different vegetative surfaces. This experimental design modified from Kuraji et al. (2001), allows for the precise quantification of branchflow and stemflow chemistry for each vertical layer of the canopy. Vertical sections of both tree stands were categorized into two compartments: (1) the canopy compartment, which is the sum of branchflow layers above the upper-stemflow collar; and (2) the trunk compartment, which is below the upper-stemflow collector to the lower-stemflow collector.

2.4. Radiocesium measurements in branchflow and stemflow

The collected branchflow and stemflow samples were filtered through a 100-μm stainless steel mesh to remove particulates >100 μm in diameter. Because this study measured and quantified dissolved radiocesium as well as particulates ≤100 μm in diameter, this research reports on the transport and flux of both dissolved and particulate radiocesium, although dissolved accounted for the vast proportion of the flux, more than 80% (Schimmack et al., 1993; Sasaki et al., 2016). After filtration, the samples were packed in 100-mL U8 type plastic containers (Yamayu Co., Ltd., Osaka, Japan) for radioactivity measurements. The determination of radiocesium in the samples was measured using a high-purity n-type germanium co-axial gamma-ray detector (EGC25-195-R, Canberra-Eurisys, Meriden, CT, USA), coupled with an amplifier (PSC822, Canberra-Eurisys, Meriden, CT, USA), and a multichannel analyzer (DSA1000, Canberra, France). The energies of gamma-ray emissions were set at peaks of 662 keV (^{137}Cs) and 605 keV (^{134}Cs). Counting time for detection of each sample for branchflow ranged from approximately three days to one week while stemflow was 24 h. A longer detection time was required for branchflow samples due to a lower ^{137}Cs concentration than stemflow samples to ensure the relative error remained less than 10%. All the measurements of radiocesium were corrected for radioactive decay between the time of sample collection and the time of radiation detection. The specific details of the measurement procedure are detailed in Kato et al. (2017).

2.5. Outer bark sampling and radiocesium measurement

Outer bark was sampled from the cedar and oak stands between 2011 and 2019. The data of outer bark from the 2011 to 2016 was previously reported by Kato et al. (2017) and Kato et al. (2019b), while subsequent data was acquired in the present study (2017–2019). The outer bark samples (~10 cm^2) were collected at about 1.3 m above the ground. The samples were oven dried for over 12 h at 105 °C before being ground into a fine powder for homogenization prior to packaging into 100-mL U8 type plastic containers (Yamayu Co., Ltd., Osaka, Japan). The determination of radiocesium in the samples was measured using a high-purity n-type germanium co-axial gamma-ray detector (EGC25-195-R, Canberra-Eurisys, Meriden, CT, USA), coupled with an amplifier (PSC822, Canberra-Eurisys, Meriden, CT, USA), and a multichannel analyzer (DSA1000, Canberra, France). The energies of gamma-ray emissions were set at peaks of 662 keV (^{137}Cs) and 605 keV (^{134}Cs). Counting time for detection of each sample was set to 3–24 h to obtain ^{137}Cs concentrations with relative errors of <10%. The determination of radiocesium activity in the samples follows the methodology employed by Kato et al. (2017), where the ^{137}Cs concentration of a dry-weight basis was expressed as Bq kg^{-1}.

2.6. Branchflow and stemflow computations

2.6.1. Depth equivalents of branchflow and stemflow

Branchflow and stemflow depth per unit basal area (L m^{-2}) was calculated as:

$$SF_{depth} = \frac{V_{SF}}{B} \quad (1)$$

where V_{SF} is a combined total volume of stemflow and branchflow in a tree stand in liters, and B is trunk basal area in m^2 (Levia and Germer, 2015).

2.6.2. ^{137}Cs concentrations via branchflow and stemflow

The ^{137}Cs concentrations in branchflow and stemflow were measured for each individual collector at each tree height and canopy position. The volume-weighted mean of ^{137}Cs concentrations of the branchflow or stemflow in each tree section, $C_{SF,\ VW}$, in Bq L^{-1} was determined as follows:

$$C_{SF,VW} = \sum_{i=1}^{n} \frac{(C_{SF} \times V_{SFcollector}) + \ldots (C_{SF} \times V_{SFcollector})_{n+1}}{V_{totalsection}} \quad (2)$$

where C_{SF} is the ^{137}Cs concentration of an individual branchflow or stemflow in n collector, (Bq L^{-1}), $V_{SFcollector}$ is the generated volume in the individual branchflow or stemflow of n collector (L), and $V_{totalsection}$ is the total volume in the tree section (L) of the monitoring period.

2.6.3. ^{137}Cs depositional flux

The ^{137}Cs depositional flux, DF_{Cs}, in Bq m^{-2} (with respect to basal area, as an approximation of the area over which stemflow is channeled to the forest floor) for each tree section was calculated as:

$$DF_{Cs} = C_{SF,VW} \times SF_{depth} \quad (3)$$

where, $C_{SF,\ VW}$ is the volume-weighted mean of ^{137}Cs concentrations of the branchflow or stemflow (Bq L^{-1}) and SF_{depth} is the stemflow depth per unit basal area (L m^{-2}). The total ^{137}Cs depositional flux per tree was computed by summing the values of each tree section for each monitoring period. Using mean total radiocesium stand fluxes per rain day, the annual fluxes are based on the cumulative number of rain days at the two monitoring sites (118 and 91 rain days for the cedar and oak stands, respectively).

For the calculations, the canopy compartment was constituted by the sum of younger foliage, mixed foliage, dead foliage and upper stemflow for cedar stand; and upper foliage, middle foliage and upper stemflow for the oak stand. The trunk compartment is composed of the lower stemflow.

3. Results

3.1. Vertical variability of ^{137}Cs flux via branchflow and stemflow

The mean and ranges of branchflow volume generated from the cedar stands through younger foliage (BF-YF), mixed foliage (BF-MF) and dead foliage (BF-DF) were 0.18 L (ranging from 0 to 0.36 L), 0.15 L (ranging from 0 to 0.27 L) and 0.11 L (ranging from 0.01 to

0.24 L), respectively. Upper stemflow (SF-U) and lower stemflow (SF-L) for cedar averaged 8.60 L (ranging from 0.28 to 20.50 L) and 4.41 L (ranging from 0.10 to 4.41 L), respectively. Total volume generated by branchflow and stemflow during the study period for individual trees Cedar A, B, and C was 129.7 L, 133.5 L and 323.7 L, respectively. In contrast, the mean and ranges of branchflow volume generated from two oak trees from upper foliage (BF-UF) and middle foliage (BF-MF) were 0.12 L (ranging from 0 to 0.30 L) and 9.43 L (ranging from 0.36 to 23.0 L), respectively. Upper stemflow (SF-U) and lower stemflow (SF-L) volumes were 23.8 L (ranging from 11.0 to 37.0 L) and 7.9 L (ranging from 0 to 28.25 L), respectively. Total branchflow and stemflow volume generated during the study period for Oak 1 and Oak 3 were 378.7 L and 633.8 L, respectively (see Fig. 3).

Fig. 4 summarizes the vertical distribution of ^{137}Cs concentrations via branchflow and stemflow of cedar and oak stands. Throughout the study period, the mean ^{137}Cs concentration in branchflow from dead foliage of the three cedar trees (1.97 ± 2.19 Bq L^{1}) was nearly seven times higher than that of the mixed foliage (0.29 ± 0.39 Bq L^{-1}) and almost thirty-three times higher than the younger foliage (0.06 ± 0.16 Bq L^{-1}). Meanwhile, the ^{137}Cs concentrations of upper stemflow (1.76 ± 1.53 Bq L^{-1}) and lower stemflow (1.43 ± 2.58 Bq L^{-1}) were practically the same for cedar. The mean ^{137}Cs concentration of branchflow from the upper foliage of the two oak trees (1.64 ± 4.16 Bq L^{-1}) was virtually the same as that of the middle foliage (1.88 ± 3.67 Bq L^{-1}). It is worth noting that the upper stemflow (3.39 ± 3.26 Bq L^{-1}) and lower stemflow (4.32 ± 4.71 Bq L^{-1}) of oak had a mean ^{137}Cs concentration approximately twice that of branchflow, with the lower stemflow having a larger mean and wider range throughout the study period.

Fig. 5 summarizes the seasonal changes of ^{137}Cs concentrations through canopy and trunk compartments in cedar and oak stands. The most striking observation from cedar was that ^{137}Cs concentrations were similar between the canopy and trunk compartments in spring but differed greatly during summer, autumn, and winter with the trunk compartment having substantially larger concentrations than the canopy. The largest concentrations of radiocesium from cedar were found in the winter for both the canopy and trunk (canopy: 1.28 Bq L^{-1}; trunk: 2.64 Bq L^{-1}). For oak, similar to cedar, the largest ^{137}Cs concentrations were found in winter. However, unlike cedar, the only season in which notable differences were observed between the canopy and trunk compartments was winter (canopy: 7.15 Bq L^{-1}; trunk: 13.66 Bq L^{-1}). The oak stand was observed to have larger ^{137}Cs concentrations in the canopy and trunk compartments than cedar over all seasons.

3.2. The relationship between ^{137}Cs concentration in stemflow and outer bark

Different trends were observed in the ^{137}Cs concentration of stemflow and ^{137}Cs concentration in outer bark for both cedar and oak

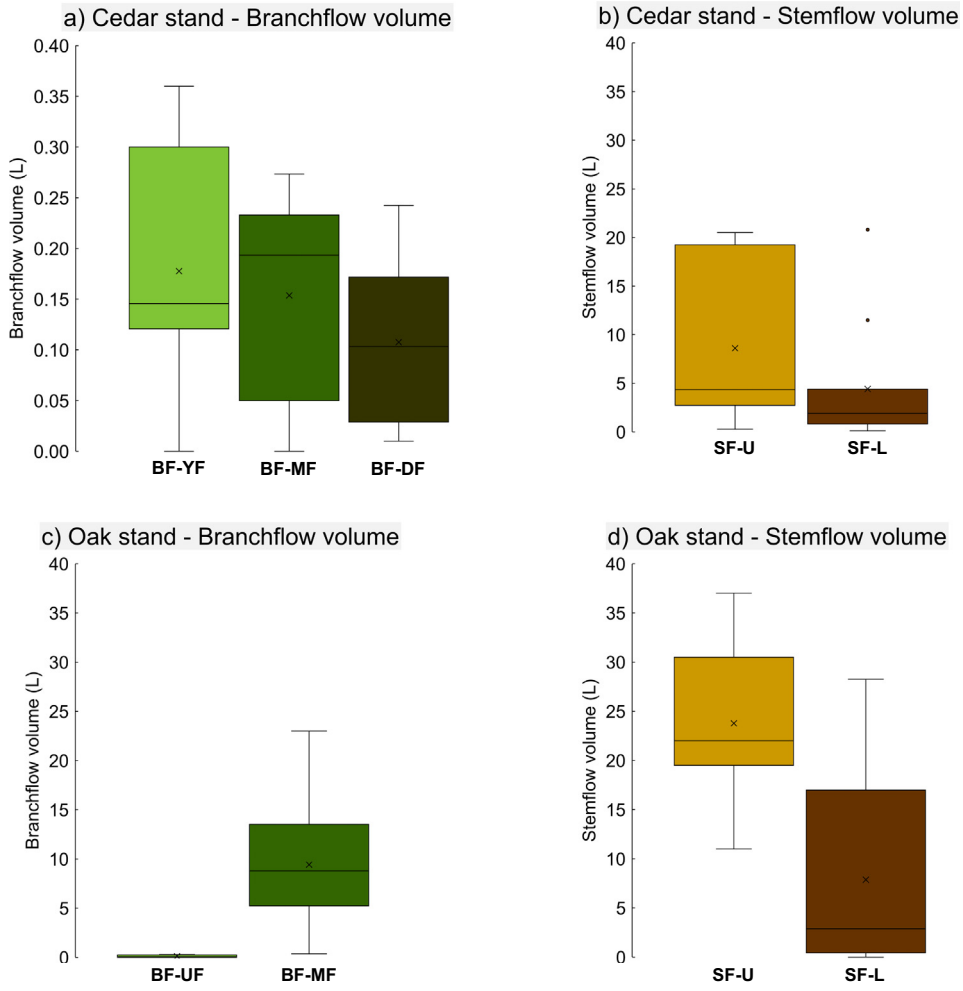

Fig. 3. Branchflow and stemflow volume for the cedar and oak stands per collection throughout the study period. Please see Fig. 2a, b for x-axis abbreviations. a) the branchflow volume in cedar stand, b) the stemflow volume in cedar stand, c) the branchflow volume in oak stand, and d) the stemflow volume in oak stand. The whiskers in the box and whisker plot show the maximum and minimum values except in the panel with outliers (shown as circles) where the whiskers denote the essential 95% of the observations. The lower and upper boundaries of the box show the 25th percentile and the 75th percentile, respectively. The cross marks indicate mean value and lines across the box indicate the median value.

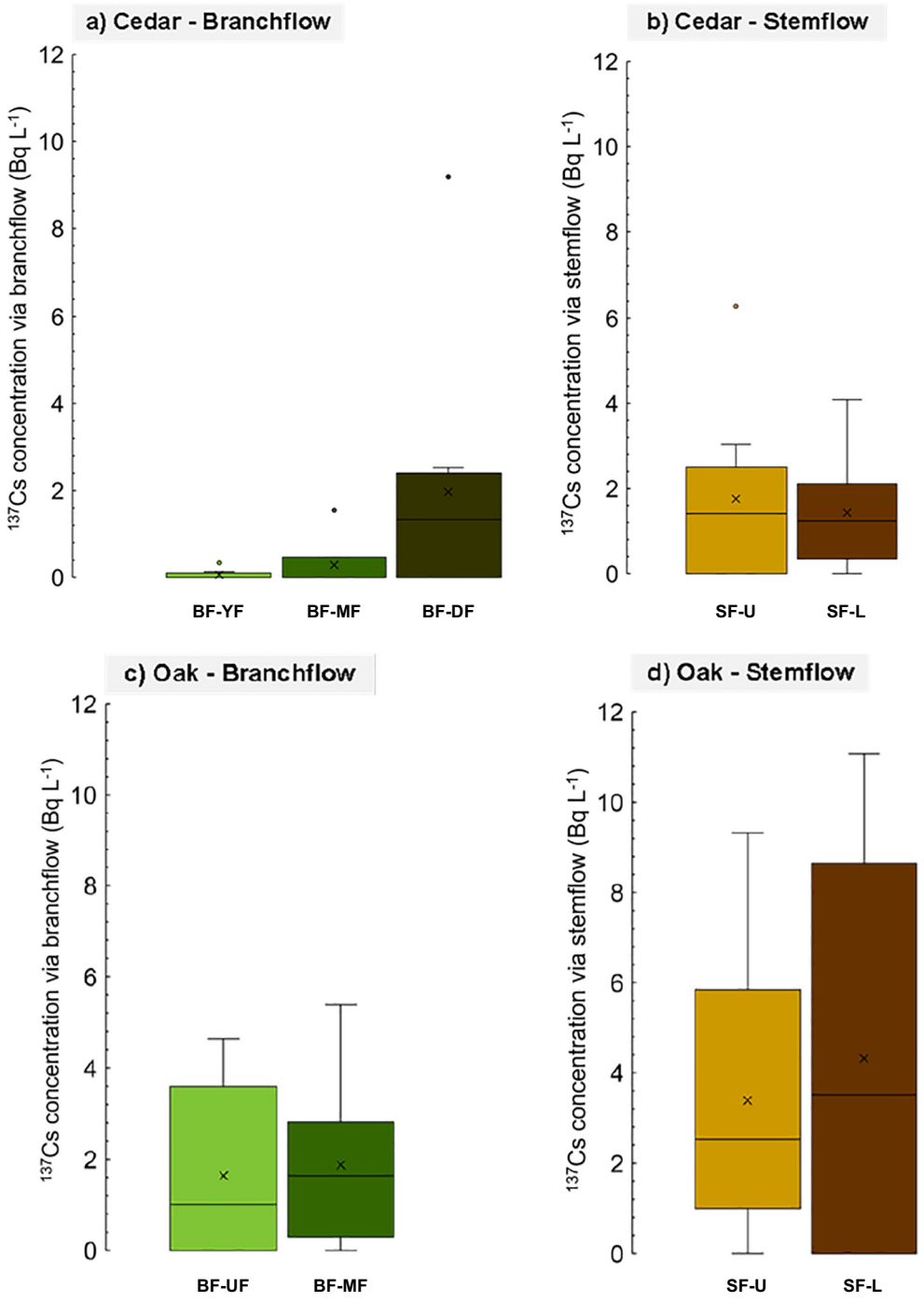

Fig. 4. The vertical distribution of volume-weighted means of ^{137}Cs concentrations in each tree compartment per collection throughout the study period. Please see Fig. 2a, b for x-axis abbreviations. a) the branchflow of cedar stand, b) the stemflow of cedar stand, c) the branchflow of oak stand, and d) the stemflow of oak stand. The whiskers in the box and whisker plot show the maximum and minimum values except in the panels with outliers (shown as circles) where the whiskers denote the essential 95% of the observations. The lower and upper boundaries of the box show the 25th percentile and the 75th percentile, respectively. The cross marks indicate mean value and lines across the box indicate the median value.

stands (Fig. 6a and b). The cedar stand showed a weak positive relationship ($SF = 11.141e^{0.0117OB}$, $R^2 = 0.03$, $p = 0.96$). In contrast, ^{137}Cs concentration in stemflow of the oak stand appears to be somewhat correlated to the ^{137}Cs concentration in the outer bark in a positive exponential trend ($SF = 7.4282e^{0.0272OB}$, $R^2 = 0.41$, $p < 0.05$).

From the trends of temporal change in Fig. 6(c) and (d), it is clear that ^{137}Cs concentrations in stemflow of both cedar and oak stands continue to decline at a steep rate with time from the nuclear accident (with linear regression for cedar stand: $SF = 38.577e^{-0.289t}$, $R^2 = 0.41$, $p < 0.05$; oak stand: $SF = 21.896e^{-0.161t}$ $R^2 = 0.22$, $p < 0.05$). Interestingly, the magnitude for ^{137}Cs concentration in the outer bark of oak stand is in a steeper and more rapid decline as compared to the cedar stand, with a slope approximately double (slope: −0.45 vs. −0.22) over time. This fact is also consistent with the exponential intercept values, where the estimated initial concentration of ^{137}Cs in the outer bark of the oak stand (84 kBq kg^{-1}) was significantly larger than that of the cedar stand (41 kBq kg^{-1}).

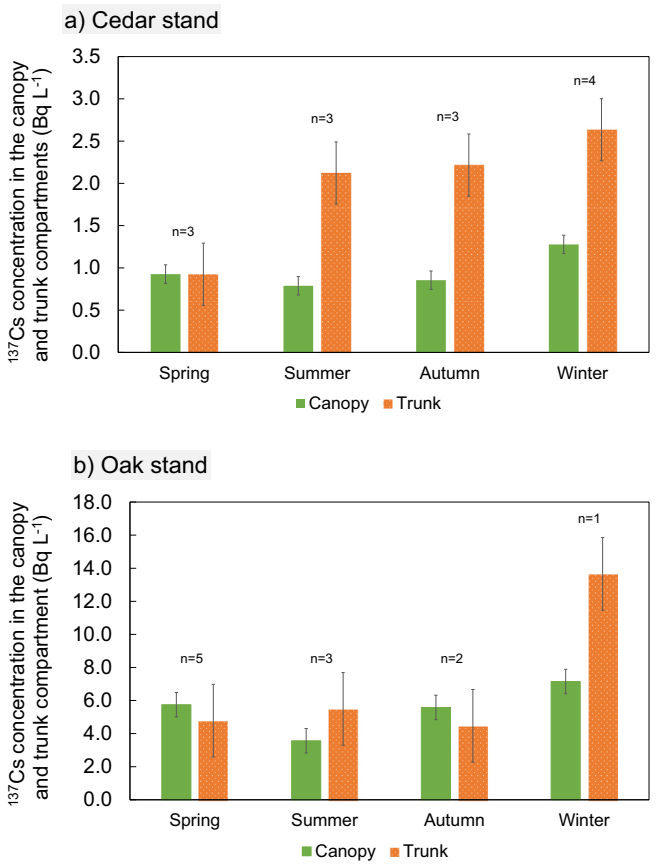

Fig. 5. Seasonal changes of ^{137}Cs concentrations of canopy and trunk compartments in cedar and oak stands among the sampled trees. Vertical bars represent the standard error of the mean. The *n* values refer to the number of collections per sampling period for each season. All test trees were sampled during each collection.

3.3. ^{137}Cs annual stemflow flux per unit trunk basal area: vertical variation and interspecific differences

Fig. 7 summarizes the ^{137}Cs depositional flux by partitioning each tree compartment via branchflow and stemflow in cedar and oak stands. Notably, nearly three-quarters of ^{137}Cs depositional flux was found to originate from the canopy of the cedar stand, while roughly equal proportions of the ^{137}Cs depositional flux was observed to originate from both the canopy and trunk compartments of the oak stand. Per unit trunk basal area, the total ^{137}Cs depositional flux for the oak stand was higher than that of the cedar stand by a factor of 7.5, with 375 and 2810 Bq m^{-2} year^{-1} for cedar stand and oak stands, respectively.

4. Discussion

4.1. Vertical variability of ^{137}Cs cycled via branchflow and stemflow

Substantial differences were found in the amounts and variability of stemflow and ^{137}Cs concentrations in branchflow and stemflow between cedar and oak stands (Figs. 3 and 4). Upper stemflow had the largest volumes as compared to branchflow or lower stemflow for both cedar and oak stands. Moreover, the ^{137}Cs concentration in the upper stemflow was the second highest for both cedar and oak stands. The high stemflow volumes and second largest radiocesium concentrations of the upper stemflow resulted in the largest ^{137}Cs flux originating from upper stemflow for the cedar stand and second largest for oak stands. For cedar, this finding implies that the upper stemflow is the point of convergence of all branchflow and stemflow from the upper canopy, with 64% of the ^{137}Cs flux being contributed solely by upper stemflow (Fig. 7). In contrast, the ^{137}Cs flux was better distributed within both upper and lower canopy portions of oak, where the upper stemflow accounted for 37% of the ^{137}Cs deposition flux and the lower stemflow 52% of the flux (Fig. 7). This finding is attributed to the tradeoff between larger volumes and ^{137}Cs concentrations between upper and lower stemflow compartments (where stemflow volume is highest for upper stemflow but ^{137}Cs concentration being highest for lower stemflow (Figs. 3 and 4)).

Our findings are congruent with previous work on the vertical variation of the stemflow generation by Hutchinson and Roberts (1981) and Kuraji et al. (2001). Intercepted rainwater channeled as stemflow was larger for upper parts of the tree. In fact, more than 98% of the stemflow was generated by the upper half of the canopy in the Douglas fir stand (Hutchinson and Roberts, 1981). Higher stemflow amounts from upper portions of tree crowns were also observed for Japanese cypress trees (Kuraji et al., 2001). Because stemflow is generated along preferred flowpaths of the tree trunk when bark water storage exceeds its capacity (Levia et al., 2010), one would expect the thinner bark of the branches and trunk of the upper parts of a tree to generate more stemflow (and more quickly) than lower portions of the tree where the bark of the trunk is thicker. Indeed, for *Pinus strobus* L. (eastern white pine), the upper portion of the tree bole was found to have a lower bark water storage capacity as a result of thinner bark, which increased with increasing height (Levia and Wubbena, 2006). As such, stemflow would usually be expected to be larger for upper portions of the tree crown, as we have found in this study.

The substantial flux of ^{137}Cs by upper stemflow suggests enhancement by foliar translocation and leaching processes. Kato et al. (2019b) also observed variation of ^{137}Cs in the vegetative samples between the tree compartments for both cedar and oak stands due to a self-decontamination process and internal recycling of ^{137}Cs, which could lead to the vertical variability of the concentration of ^{137}Cs in the stemflow observed for cedar and oak in this study. For cedar, branchflow from dead foliage at the bottom of the canopy had a larger ^{137}Cs concentration than other branchflow types in the upper canopy of cedar stands. Generally, branchflow from younger and mixed foliage have been shown to have ^{137}Cs concentrations below the detection limit. We believe that some non-detectable ^{137}Cs concentrations in the branchflow from younger and mixed foliage may be due to the foliar leaching process and translocation of ^{137}Cs from vegetative tissues (living needles and branches). Older needles were more likely to translocate the ^{137}Cs to newer foliage such as needle, male flower and pollen in the cedar stand (Yoshihara et al., 2014; Kanasashi et al., 2015). As the foliage in the cedar stand lasts more than a single year, the radiocesium in aging needles can be translocated to greener needles on the crown periphery (Hara et al., 2020). Moreover, beyond the forest studied, it is important to note that ^{137}Cs can be incorporated with pollen and mixed with other bioaerosols, which could expose humans to anthropogenic radioactive particles at locations further away, as partially governed by prevailing meteorological and atmospheric conditions (Bunzl et al., 1993; Kita et al., 2020; Kiyono et al., 2020).

Significant differences in the vertical variation of branchflow and stemflow of the tree stands' compartments among trees in the plot and between cedar and oak species may partly be due to differential interception of radiocesium soon after the FDNPP accident. Canopy interception of the total deposition was 70% for cedar forest and only 20% for broadleaved forest (Kato et al., 2017). The oak trees were leafless when the nuclear accident occurred but the cedar trees were not, thus radiocesium was intercepted by both foliar and woody surfaces in the cedar canopy and only the leafless crowns of the oak trees. These differences might be explained, at least partly, by either the concentration of ^{137}Cs retained in each portion of the tree canopy vis-à-vis the different flowpaths of stemflow through the canopy, or by the differential residence times and path lengths of the branchflow (shorter) and stemflow

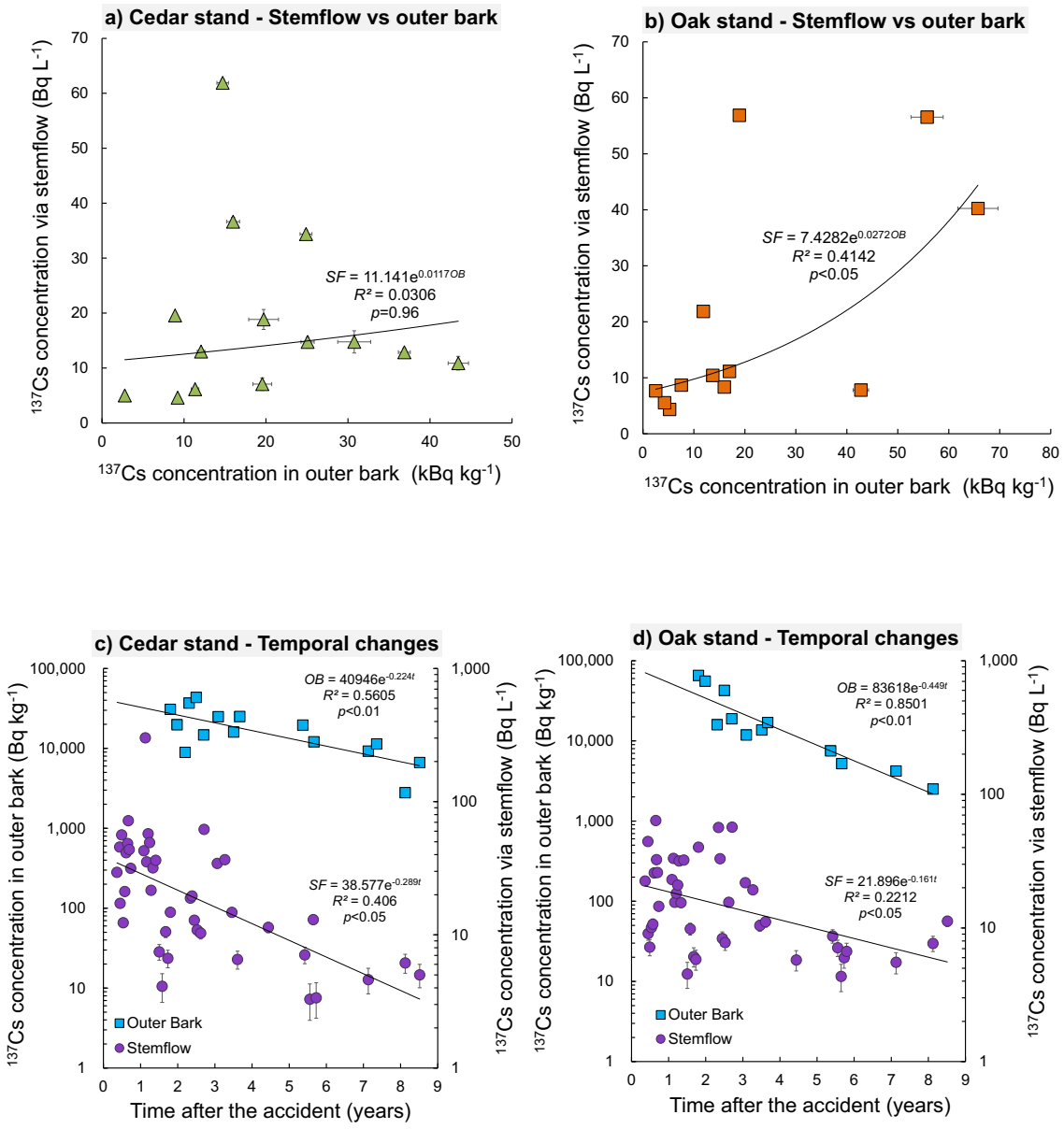

Fig. 6. The relationship between ^{137}Cs concentrations in stemflow and outer bark for a) cedar stand; and b) oak stand. Temporal changes in the ^{137}Cs concentrations of stemflow and outer bark for c) cedar stand; and d) oak stand. Error in the ^{137}Cs concentration represents a standard deviation for the measured ^{137}Cs concentration in multiple samples. The period of monitoring data was from 2011 to 2019. The data from the 2011 to 2016 periods was previously reported by Kato et al. (2017) and Kato et al. (2019b), while subsequent data was from the present study (2017–2019).

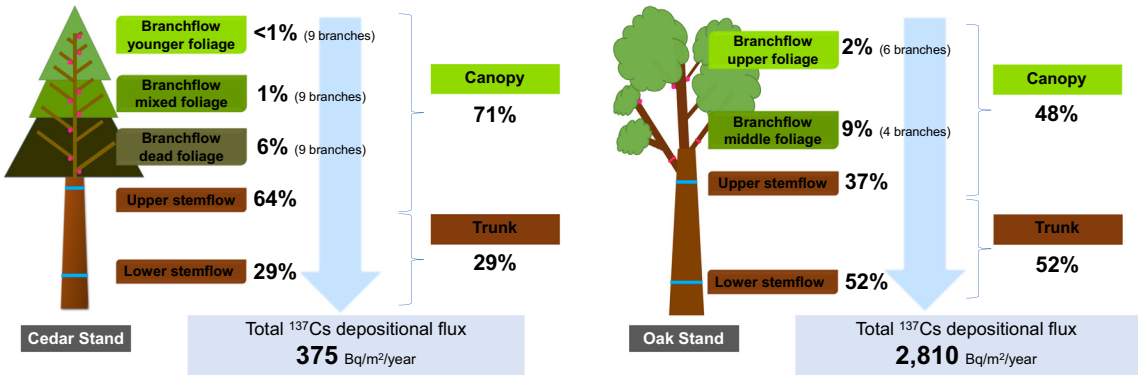

Fig. 7. Schematic diagram summarizing the vertical and total ^{137}Cs depositional flux per unit trunk basal area via branchflow and stemflow in cedar and oak stands. The annual fluxes are based on the cumulative number of rain days at the two monitoring sites (118 and 91 rain days for the cedar and oak stands, respectively).

(longer) over the woody frames of the trees. Hence, a longer flowpath may increase the probability of dissolution of ^{137}Cs materials. Given the verticality of radiocesium cycling observed in this study (Fig. 7), and the importance of upper stemflow (representing the canopy), we contend that one should not simply average stemflow fluxes collected from the tree base to compute radiocesium stocks in the forest, otherwise the stores of radiocesium in the upper canopy will be missed and lead to overall underestimates of radiocesium stocks within the trees.

4.2. Seasonal changes of ^{137}Cs cycling in canopy and trunk

We observed significant changes in ^{137}Cs concentration due to seasonal variations in the canopy and trunk compartments for both the cedar and oak stands (Fig. 5). For cedar, ^{137}Cs concentrations were always larger from the trunk than the canopy compartment, especially during summer, autumn, and winter. The difference, however, was most pronounced in winter. For oak, the trunk compartment had higher concentrations than the canopy during summer and winter, with the largest difference appearing in winter. These results highlight the importance of winter leaching from the tree trunk. While these initial findings are noteworthy, one must recognize the small sample size and regard these findings with season as preliminary. Neary and Gizyn (1994) also found stemflow leaching from bark surfaces was notable during winter, where K^+ losses were largest from the leafless deciduous trees. Storm conditions, such as intensity and air temperature, will also impact the extent of winter stemflow leaching (Levia, 2003; Staelens et al., 2007). The influence of varying precipitation types among seasons, where the summer has a significant proportion of convective precipitation and winter has frontal precipitation, can generate significantly different stemflow volumes and alter stemflow solute inputs (Levia and Frost, 2003). Further study needs to address the influence of increased contact time of stemflow on the bark with lower air temperatures and viscosity (Levia and Herwitz, 2000) as well as any influence of snowmelt-induced stemflow (Levia and Underwood, 2004) on the leaching and transport of radiocesium during winter.

4.3. ^{137}Cs cycling via branchflow and stemflow

The direct atmospheric deposition of ^{137}Cs to the foliage and outer bark of cedar and oak stands results in the direct uptake and storage of ^{137}Cs within the trees due to rapid translocation (Thiry et al., 2016; Yoshihara et al., 2016; Imamura et al., 2017a; Kato et al., 2019b). The stored ^{137}Cs is later leached or washed by the precipitation via branchflow and stemflow. The tendency of ^{137}Cs to be released or retained by the foliage and outer bark via branchflow and stemflow results in storm, seasonal, and annual scale patterns of ^{137}Cs flux.

From Fig. 6a and c, it is apparent that ^{137}Cs could be sequestered by the vegetation in the cedar stand (particularly in the trunk) with a relatively constant relationship between ^{137}Cs concentration in stemflow and outer bark detected over nine years after the accident. The observed relationship for cedar may be due to the attainment of a solubility equilibrium threshold being reached between stemflow and the bark, suggesting that soluble ^{137}Cs incorporated inside the tree tends to leach (Nimis, 1996) and is therefore biologically available within the tree stand. In contrast, particulate ^{137}Cs is heterogeneously distributed on the bark surface (Sasaki et al., 2016). The decreasing trend of ^{137}Cs concentration in the bark of cedar stands indicates decontamination through the leaching process from bark to stemflow and the debarking process (Ohashi et al., 2017), whereby the older bark is peeled-off together with the ^{137}Cs (through debarking process) and the ^{137}Cs located within the now-exposed inner bark was transported by stemflow during precipitation (via leaching). Crockford et al. (1996) reported that the exposed surface of the new bark and detached bark pieces are the sources of cations, which increased the stemflow concentrations. However, the washoff and debarking rates of the bark were assumed to be slower than in needles and branches (Imamura et al., 2017b), although this study found that the canopy could be a more dominant source of ^{137}Cs than the trunk via the leaching of ^{137}Cs by branchflow and stemflow. We suspect that the ^{137}Cs appeared to be washoff and migrated from the upper to the lower part of the canopy (since the ^{137}Cs concentration was detected in smaller amount in the branchflow of younger foliage and the larger contribution from branchflow of dead foliage) and then converged onto the trunk. Therefore, ^{137}Cs was readily accessible and remained in steady supply from the canopy, subsequently being cycled on the trunk.

In contrast, a different process appears to be occurring in the oak stand (Fig. 6(b) and (d)), where the ^{137}Cs leaching process was taking place mainly within the trunk with a higher contribution of ^{137}Cs concentration in stemflow with an increase of ^{137}Cs concentration in the outer bark (Fig. 6(b)) relative to its temporal changes over the nine years of the accident (Fig. 6(d)). The ^{137}Cs uptake into the newly developed oak leaves possibly occurred through the outer bark surfaces of the stems, branches, and twigs, rather than through foliar uptake (Kato et al., 2019b). A higher concentration of ^{137}Cs via stemflow with the main form being dissolved also has been observed in previous studies. Sasaki et al. (2016) found a higher concentration of ^{137}Cs via stemflow from Japanese chestnut with the main form being dissolved ^{137}Cs, with an average of 10 Bq L^{-1}. Meanwhile, the ratio of dissolved radiocesium to particulate radiocesium was about 10 in the stemflow (Schimmack et al., 1993). We contend that radiocesium fractionation (particulate and dissolved) varies and fluctuates in relation to bark condition (e.g., morphology, water repellency, water storage capacity, maturity of outer bark), which, in turn, causes significant variability of ^{137}Cs over time. A high incorporation rate by the elution of dissolved ^{137}Cs from bark to the stemflow (Fig. 6b) resulted in a rapid decline of ^{137}Cs in the outer bark of the oak stand (Fig. 6d) as compared to the cedar stand (Fig. 6c). Because bark is easily leached (Neary and Gizyn, 1994), a decrease of ^{137}Cs concentration in the outer bark implies that the ^{137}Cs solutes leached from the bark into branchflow and stemflow, thus creating the declining pattern of ^{137}Cs in the outer bark and enrichment of the 'trunk compartment' samples with ^{137}Cs via stemflow during summer and winter (Fig. 5). It is plausible that the solute leaching of radiocesium and transport from the bark is governed, at least partially, by volumetric flow rates on the bark surface, wetted perimeters, water sources and sinks (e.g., evaporation and direct rain input), bark water storage, and solute concentrations (Tucker et al., 2020). Because ^{137}Cs concentrations were relatively high in bark compared to other biomass compartments, even after six years (Kato et al., 2019b) and 22 years after the CNPP accident (Zhiyanski et al., 2010), it represents an appreciable source of radiocesium for decades.

The annual total ^{137}Cs depositional flux for the oak stand was 7.5 times higher than that of the cedar stand (Fig. 7). This fact may be partly attributed to the variation in water storage capacity at the vegetative cover and trunk of both species, hence contributing to the different input volumes and ^{137}Cs concentration in the branchflow and stemflow. Furthermore, we observed a larger ^{137}Cs depositional flux from the dead foliage (6%) than living foliage (less than 2%), possibly due to the lesser ability of the dead foliage to generate branchflow. Nearly 40–50% of the residual ^{137}Cs in the canopy were attributed to the dead needles and branches with two times the ^{137}Cs inventory (43.39 kBq m^{-2}) than the living needles and branches (21.91 kBq m^{-2}) (Coppin et al., 2016).

The next questions emerging from this study include how water storage capacity and precipitation partitioning in tree stand could influence the transport of radiocesium (mainly dissolved ^{137}Cs) along the stemflow flowpath. A fruitful approach may be to adapt the network solute transport model for stemflow developed by Tucker et al. (2020) that addresses some of the intricacies of the physico-chemical dynamics operating within tree bark. Using a physically-based mathematical approach, it may be possible to integrate bark water storage capacity, stemflow production, and radiocesium flux vertically. A successful model of radiocesium cycling (employing concentration and flux data in this study, Table S2) could be used to forecast deposition rates to

near-trunk soils and allow researchers to pinpoint which parts of trees are contributing disproportionate shares of radiocesium to the forest soil.

5. Conclusions

This study clarified the vertical variability of radiocesium cycling via branchflow and stemflow through the canopies of cedar and oak stands in the aftermath of the FDNPP accident. We investigated the fate of radiocesium transported by branchflow from upper and lower portions of the canopy and deposited by stemflow at trunk-base. We draw the following conclusions:

1. Significant differences in branchflow and stemflow production and ^{137}Cs concentrations were detected for both tree species in relation to vertical position along the tree profile. While water flowpaths through canopies are complex, these results might be partly attributed to the differences in flowpath routing between branchflow (shorter flowpath) and stemflow (longer flowpath) and their corresponding residence times.
2. ^{137}Cs concentrations in branchflow and stemflow were largest during winter.
3. 71% and 48% of the ^{137}Cs flux originated from cedar/oak upper canopies, respectively. The ^{137}Cs depositional flux was roughly equal between the canopy (48%) and trunk (52%) compartments for oak, while the differences were much more pronounced for cedar with the canopy accounting for 71% of the radiocesium flux and the trunk 29%.
4. The annual ^{137}Cs flux from the oak stand was 7.5 times greater than cedar due to differences in tree morphology and biomass and capture of radiocesium substances during initial fallout.

Results from this project may be used by biogeochemists, foresters, hydrologists, and other scientists and planners to better understand the origin and variation of radiocesium fluxes on trees as well as the magnitude of near-trunk radiocesium fluxes to forest soils. Once these empirical results are coupled with a physically-based model, researchers and planners will be able to better predict areas of chronic radiation exposure in future scenarios, and therefore create more specific boundaries and timing for exclusion zones.

CRediT authorship contribution statement

Zul Hilmi Saidin: Conceptualization, Methodology, Validation, Formal analysis, Investigation, Data curation, Writing - original draft, Visualization. **Delphis F. Levia**: Conceptualization, Writing - review & editing. **Hiroaki Kato**: Conceptualization, Validation, Investigation, Writing - review & editing, Supervision. **Momo Kurihara**: Validation, Writing - review & editing. **Janice E. Hudson**: Validation, Writing - review & editing. **Kazuki Nanko**: Writing - review & editing. **Yuichi Onda**: Conceptualization, Validation, Resources, Writing - review & editing, Supervision, Project administration, Funding acquisition.

Declaration of competing interest

The authors declare that they have no known competing financial interests or personal relationships that could have appeared to influence the work reported in this paper.

Acknowledgements

This work was conducted as a commissioned study from the Japan Atomic Energy Agency, as a part of the Ministry of Education, Culture, Sports, Science and Technology-funded FY2011–2012, and the Nuclear Regulation Authority of Japan-funded FY 2012–2014, as well as the Japan Atomic Energy Agency-funded FY2015–2016, FY2017-2018. This work was further supported by Environmental Radioactivity Research Network Center (I-20-02) awarded to DFL. In addition, this work was partially supported by a Grant-in-Aid for Scientific Research on Innovative Areas (Research in a proposed research area; #15H00969 and #2411006) from the Japan Society for the Promotion of Science. ZHS would like to thank the Ministry of Education, Culture, Sports, Science and Technology (MEXT), Japan for his study scholarship.

Appendix A. Supplementary data

Supplementary data to this article can be found online at https://doi.org/10.1016/j.scitotenv.2021.151698.

References

Adachi, K., Kajino, M., Zaizen, Y., Igarashi, Y., 2013. Emission of spherical cesium-bearing particles from an early stage of the Fukushima nuclear accident. Sci. Rep. 3. https://doi.org/10.1038/srep02554.

Bunzl, K., Hötzl, H., Winkler, R., 1993. Spruce pollen as a source of increased radiocesium concentrations in air. Naturwissenschaften 80, 173–174. https://doi.org/10.1007/BF01226376.

Carlyle-Moses, D.E., Iida, S., Germer, S., Llorens, P., Michalzik, B., Nanko, K., Tischer, A., Levia, D.F., 2018. Expressing stemflow commensurate with its ecohydrological importance. Adv. Water Resour. https://doi.org/10.1016/j.advwatres.2018.08.015.

Chino, M., Nakayama, H., Nagai, H., Terada, H., Katata, G., Yamazawa, H., 2011. Preliminary estimation of release amounts of ^{131}I and ^{137}Cs accidentally discharged from the Fukushima Daiichi nuclear power plant into the atmosphere. J. Nucl. Sci. Technol. 48, 1129–1134. https://doi.org/10.3327/jnst.48.1129.

Coppin, F., Hurtevent, P., Loffredo, N., Simonucci, C., Julien, A., Gonze, M.-A., Nanba, K., Onda, Y., Thiry, Y., 2016. Radiocaesium partitioning in Japanese cedar forests following the "early" phase of Fukushima fallout redistribution. Sci. Rep. 6, 37618. https://doi.org/10.1038/srep37618.

Crockford, R.H., Richardson, D.P., Sageman, R., 1996. Chemistry of rainfall, throughfall and stemflow in a eucalypt forest and a pine plantation in south-eastern Australia: 3. Stemflow and total inputs. Hydrol. Process. https://doi.org/10.1002/(SICI)1099-1085(199601)10:1<25::AID-HYP297>3.0.CO;2-W.

Endo, I., Ohte, N., Iseda, K., Tanoi, K., Hirose, A., Kobayashi, N.I., Murakami, M., Tokuchi, N., Ohashi, M., 2015. Estimation of radioactive 137-cesium transportation by litterfall, stemflow and throughfall in the forests of Fukushima. J. Environ. Radioact. 149, 176–185. https://doi.org/10.1016/j.jenvrad.2015.07.027.

Forster, H., Schimmack, W., 1992. Influence of the stemflow on the depth distribution of radiocesium in the soil under a beech stand. Naturwissenschaften https://doi.org/10.1007/BF01132274.

Geras'kin, S., Volkova, P., Vasiliyev, D., Dikareva, N., Oudalova, A., Kazakova, E., Makarenko, E., Duarte, G., Kuzmenkov, A., 2019. Scots pine as a promising indicator organism for biomonitoring of the polluted environment: a case study on chronically irradiated populations. Mutat. Res. Toxicol. Environ. Mutagen. 842, 3–13. https://doi.org/10.1016/J.MRGENTOX.2018.12.011.

Guo, L., Mount, G.J., Hudson, S., Lin, H., Levia, D., 2020. Pairing geophysical techniques improves understanding of the near-surface critical zone: visualization of preferential routing of stemflow along coarse roots. Geoderma https://doi.org/10.1016/j.geoderma.2019.113953.

Hara, T., Takenaka, C., Tomioka, R., 2020. Change in the chemical form of ^{137}Cs with age in needles of Japanese cedar. J. Environ. Radioact. 213, 106137. https://doi.org/10.1016/J.JENVRAD.2019.106137.

Hirose, K., 2012. 2011 Fukushima Dai-ichi nuclear power plant accident: summary of regional radioactive deposition monitoring results. J. Environ. Radioact. 111, 13–17. https://doi.org/10.1016/j.jenvrad.2011.09.003.

Hutchinson, I., Roberts, M.C., 1981. Vertical variation in stemflow generation. J. Appl. Ecol. 18, 521–527. https://doi.org/10.2307/2402413.

IAEA, 2006. Environmental Consequences of the Chernobyl Accident and their Remediation: Twenty Years of Experience. Report of the Chernobyl Forum Expert Group 'Environment'. Radiological Assessment Reports Series. International Atomic Energy Agency, Vienna. https://www.iaea.org/publications/7382/environmental-consequences-of-the-chernobyl-accident-and-their-remediation-twenty-years-of-experience https://www-pub.iaea.org/MTCD/Publications/PDF/Pub1239_web.pdf.

Imamura, N., Komatsu, M., Ohashi, S., Hashimoto, S., Kajimoto, T., Kaneko, S., Takano, T., 2017a. Temporal changes in the radiocesium distribution in forests over the five years after the Fukushima Daiichi Nuclear Power Plant accident. Sci. Rep. https://doi.org/10.1038/s41598-017-08261-x.

Imamura, N., Levia, D.F., Toriyama, J., Kobayashi, M., Nanko, K., 2017b. Stemflow-induced spatial heterogeneity of radiocesium concentrations and stocks in the soil of a broadleaved deciduous forest. Sci. Total Environ. 599, 1013–1021. https://doi.org/10.1016/j.scitotenv.2017.05.017.

Kanasashi, T., Sugiura, Y., Takenaka, C., Hijii, N., Umemura, M., 2015. Radiocesium distribution in sugi (*Cryptomeria japonica*) in Eastern Japan: translocation from needles to pollen. J. Environ. Radioact. https://doi.org/10.1016/j.jenvrad.2014.06.018.

Kaneyasu, N., Ohashi, H., Suzuki, F., Okuda, T., Ikemori, F., 2012. Sulfate aerosol as a potential transport medium of radiocesium from the Fukushima nuclear accident. Environ. Sci. Technol. https://doi.org/10.1021/es204667h.

Kato, H., 2020. Radiocesium Cycling in the Context of Forest-Water Interactions, pp. 371–393 https://doi.org/10.1007/978-3-030-26086-6_16.

Kato, H., Onda, Y., 2018. Determining the initial Fukushima reactor accident-derived cesium-137 fallout in forested areas of municipalities in Fukushima Prefecture. J. For. Res. 23, 73–84. https://doi.org/10.1080/13416979.2018.1448566.
Kato, H., Onda, Y., Nanko, K., Gomi, T., Yamanaka, T., Kawaguchi, S., 2013. Effect of canopy interception on spatial variability and isotopic composition of throughfall in Japanese cypress plantations. J. Hydrol. 504, 1–11. https://doi.org/10.1016/J.JHYDROL.2013.09.028.
Kato, H., Hisadome, K., Loffredo, N., Kawamori, A., 2017. Temporal changes in radiocesium deposition in various forest stands following the Fukushima Dai-ichi Nuclear Power Plant accident. J. Environ. Radioact. 166, 449–457. https://doi.org/10.1016/J.JENVRAD.2015.04.016.
Kato, H., Onda, Y., Gao, X., Sanada, Y., Saito, K., 2019a. Reconstruction of a Fukushima accident-derived radiocesium fallout map for environmental transfer studies. J. Environ. Radioact. 210, 105996. https://doi.org/10.1016/j.jenvrad.2019.105996.
Kato, H., Saidin, Z.H., Sakashita, W., Hisadome, K., Loffredo, N., 2019b. Six-year monitoring study of radiocesium transfer in forest environments following the Fukushima nuclear power plant accident. J. Environ. Radioact. 210, 105817. https://doi.org/10.1016/j.jenvrad.2018.09.015.
Kinoshita, N., Sueki, K., Sasa, K., Ikarashi, S., Nishimura, T., Wong, Y.-S., Satou, Y., Handa, K., Takahashi, T., Sato, M., Yamagata, T., Kitagawa, J.-i., 2011. Assessment of individual radionuclide distributions from the Fukushima nuclear accident covering central-east Japan. Proc. Natl. Acad. Sci. https://doi.org/10.1073/pnas.1111724108.
Kita, K., Igarashi, Y., Kinase, T., Hayashi, N., Ishizuka, M., Adachi, K., Koitabashi, M., Sekiyama, T.T., Onda, Y., 2020. Rain-induced bioecological resuspension of radiocaesium in a polluted forest in Japan. Sci. Rep. 10, 1–15. https://doi.org/10.1038/s41598-020-72029-z.
Kiyono, Y., Akama, A., Kanazashi, T., Shichi, K., Kondo, T., Hoshi, H., Kuramoto, N., Fujisawa, Y., Kuramoto, S., 2020. ^{137}Cs concentrations in the pollen of sugi (*Cryptomeria japonica* var. *japonica*) over 5 years following the 2011 Fukushima Daiichi Nuclear Power Station accident in Fukushima Prefecture. 森林総合研究所研究報告 (Bulletin of FFPRI) 19 (1), 89–104. https://doi.org/10.20756/ffpri.19.1_89.
Koizumi, A., Niisoe, T., Harada, K.H., Fujii, Y., Adachi, A., Hitomi, T., Ishikawa, H., 2013. ^{137}Cs trapped by biomass within 20 km of the Fukushima Daiichi Nuclear Power Plant. Environ. Sci. Technol. 47, 9612–9618. https://doi.org/10.1021/es401422g.
Kuraji, K., Tanaka, Y., Tanaka, N., Karakama, I., 2001. Generation of stemflow volume and chemistry in a mature Japanese cypress forest. Hydrol. Process. 15, 1967–1978. https://doi.org/10.1002/hyp.250.
Kurihara, M., Onda, Y., Suzuki, H., Iwasaki, Y., Yasutaka, T., 2018. Spatial and temporal variation in vertical migration of dissolved ^{137}Cs passed through the litter layer in Fukushima forests. J. Environ. Radioact. 192. https://doi.org/10.1016/j.jenvrad.2018.05.012.
Levia, D.F., 2003. Winter stemflow nutrient inputs into a southern New England broadleaved deciduous forest. 1st ed. Geogr. Ann. Ser. B85. Taylor & Francis, Ltd... https://www.jstor.org/stable/3566178.
Levia, D.F., Frost, E.E., 2003. A review and evaluation of stemflow literature in the hydrologic and biogeochemical cycles of forested and agricultural ecosystems. J. Hydrol. 274, 1–29. https://doi.org/10.1016/S0022-1694(02)00399-2.
Levia, D.F., Germer, S., 2015. A review of stemflow generation dynamics and stemflow-environment interactions in forests and shrublands. Rev. Geophys. 53, 673–714. https://doi.org/10.1002/2015RG000479.
Levia, D.F., Herwitz, S.R., 2000. Physical properties of water in relation to stemflow leachate dynamics: implications for nutrient cycling. Can. J. For. Res. 30 (4), 662–666. https://doi.org/10.1139/x99-244.
Levia, D.F., Underwood, S.J., 2004. Snowmelt induced stemflow in northern hardwood forests: a theoretical explanation on the causation of a neglected hydrological process. Adv. Water Resour. 27, 121–128. https://doi.org/10.1016/j.advwatres.2003.12.001.
Levia, D.F., Wubbena, N.P., 2006. Vertical variation of bark water storage capacity of *Pinus strobus* L. (eastern white pine) in Southern Illinois. Northeast. Nat. 13 (1), 131–137. https://doi.org/10.1656/1092-6194(2006)13[131:VVOBWS]2.0.CO;2.
Levia, D.F., Van Stan, J.T., Mage, S.M., Kelley-Hauske, P.W., 2010. Temporal variability of stemflow volume in a beech-yellow poplar forest in relation to tree species and size. J. Hydrol. 380, 112–120. https://doi.org/10.1016/j.jhydrol.2009.10.028.
Loffredo, N., Onda, Y., Kawamori, A., Kato, H., 2014. Modeling of leachable ^{137}Cs in throughfall and stemflow for Japanese forest canopies after Fukushima Daiichi Nuclear Power Plant accident. Sci. Total Environ. 493, 701–707. https://doi.org/10.1016/j.scitotenv.2014.06.059.
Loffredo, N., Onda, Y., Hurtevent, P., Coppin, F., 2015. Equation to predict the ^{137}Cs leaching dynamic from evergreen canopies after a radio-cesium deposit. J. Environ. Radioact. 147, 100–107. https://doi.org/10.1016/j.jenvrad.2015.05.018.
MEXT, 2011a. Preparation of Distribution Map of Radiation Doses, etc. (Map of Radioactive Cesium Concentration in Soil) by MEXT. radioactivity.nsr.go.jp/en/contents/5000/4165/24/1750_083014.pdf. (Accessed 4 August 2017).
MEXT, 2011b. Results of the Third Airborne Monitoring Survey by MEXT Radioactivity. nsr.go.jp/en/contents/5000/4182/24/1304797_0708e.pdf. (Accessed 4 August 2017).
Morino, Y., Ohara, T., Watanabe, M., Hayashi, S., Nishizawa, M., 2013. Episode analysis of deposition of radiocesium from the Fukushima Daiichi nuclear power plant accident. Environ. Sci. Technol. 47. https://doi.org/10.1021/es304620x.
Neary, A.J., Gizyn, W.I., 1994. Throughfall and stemflow chemistry under deciduous and coniferous forest canopies in south-central Ontario. Can. J. For. Res. 24 (6), 1089–1100. https://doi.org/10.1139/x94-145.
Niizato, T., Abe, H., Mitachi, K., Sasaki, Y., Ishii, Y., Watanabe, T., 2015. Input and output budgets of radiocesium concerning the forest floor in the mountain forest of Fukushima released from the TEPCO's Fukushima Dai-ichi nuclear power plant accident. J. Environ. Radioact. https://doi.org/10.1016/j.jenvrad.2016.04.017.
Nimis, P.L., 1996. Radiocesium in plants of forest ecosystems. Stud. Geobot. http://dbiodbs.univ.trieste.it/ecoapp/cesio.pdf.
Nishikiori, T., Watanabe, M., Koshikawa, M.K., Takamatsu, T., Ishii, Y., Ito, S., Takenaka, A., Watanabe, K., Hayashi, S., 2015. Uptake and translocation of radiocesium in cedar leaves following the Fukushima nuclear accident. Sci. Total Environ. 502, 611–616. https://doi.org/10.1016/j.scitotenv.2014.09.063.
Ohashi, S., Kuroda, K., Takano, T., Suzuki, Y., Fujiwara, T., Abe, H., Kagawa, A., Sugiyama, M., Kubojima, Y., Zhang, C., Yamamoto, K., 2017. Temporal trends in ^{137}Cs concentrations in the bark, sapwood, heartwood, and whole wood of four tree species in Japanese forests from 2011 to 2016. J. Environ. Radioact. 178–179. https://doi.org/10.1016/j.jenvrad.2017.09.008.
Onda, Y., Taniguchi, K., Yoshimura, K., Kato, H., Takahashi, J., Wakiyama, Y., Coppin, F., Smith, H., 2020. Radionuclides from the Fukushima Daiichi Nuclear Power Plant in terrestrial systems. Nat. Rev. Earth Environ. 1, 644–660. https://doi.org/10.1038/s43017-020-0099-x.
Sasaki, Y., Abe, H., Mitachi, K., Watanabe, T., Ishii, Y., Niizato, T., 2016. The transfer of radiocesium from the bark to the stemflow of chestnut trees (*Castanea crenata*) contaminated by radionuclides from the Fukushima Dai-ichi nuclear power plant accident. J. Environ. Radioact. https://doi.org/10.1016/j.jenvrad.2015.12.001.
Schimmack, Förster, Bunzl, Kreutzer, 1993. Deposition of radiocesium to the soil by stemflow, throughfall and leaf-fall from beech trees. Radiat. Environ. Biophys. 32, 137–150. https://doi.org/10.1007/BF01212800.
Staelens, J., De Schrijver, A., Verheyen, K., 2007. Seasonal variation in throughfall and stemflow chemistry beneath a European beech (*Fagus sylvatica*) tree in relation to canopy phenology. Can. J. For. Res. 37 (8), 1359–1372. https://doi.org/10.1139/X07-003.
Takahashi, J., Tamura, K., Suda, T., Matsumura, R., Onda, Y., 2015. Vertical distribution and temporal changes of ^{137}Cs in soil profiles under various land uses after the Fukushima Dai-ichi Nuclear Power Plant accident. J. Environ. Radioact. 139, 351–361. https://doi.org/10.1016/j.jenvrad.2014.07.004.
Takahashi, J., Onda, Y., Hihara, D., Tamura, K., 2019. Six-year monitoring of the vertical distribution of radiocesium in three forest soils after the Fukushima Dai-ichi Nuclear Power Plant accident. J. Environ. Radioact. 210, 105811. https://doi.org/10.1016/j.jenvrad.2018.09.009.
Tanaka, T., Taniguchi, M., Tsujimura, M., 1996. Significance of stemflow in groundwater recharge. 2: a cylindrical infiltration model for evaluating the stemflow contribution to groundwater recharge. Hydrol. Process. 10 (1), 81–88. https://doi.org/10.1002/(SICI)1099-1085(199601)10:1<81::AID-HYP302>3.0.CO;2-M (accessed 6.1.21) https://onlinelibrary.wiley.com/doi/pdf/10.1002/(SICI)1099-1085(199601)10:1%3C81::AID-HYP302%3E3.0.CO;2-M.
Taniguchi, M., Tsujimura, M., Tanaka, T., 1996. Significance of stemflow in groundwater recharge. 1: evaluation of the stemflow contribution to recharge using a mass balance approach. Hydrol. Process. 10 (1). https://doi.org/10.1002/(SICI)1099-1085(199601)10:1%3C71::AID-HYP301%3E3.0.CO;2-Q. https://onlinelibrary.wiley.com/doi/abs/10.1002/%28SICI%291099-1085%28199601%2910%3A1%3C71%3A%3AAID-HYP301%3E3.0.CO%3B2-Q.
Terada, H., Katata, G., Chino, M., Nagai, H., 2012. Atmospheric discharge and dispersion of radionuclides during the Fukushima Dai-ichi Nuclear Power Plant accident. Part II: verification of the source term and analysis of regional-scale atmospheric dispersion. J. Environ. Radioact. 112, 141–154. https://doi.org/10.1016/j.jenvrad.2012.05.023.
Teramage, M.T., Onda, Y., Patin, J., Kato, H., Gomi, T., Nam, S., 2014. Vertical distribution of radiocesium in coniferous forest soil after the Fukushima Nuclear Power Plant accident. J. Environ. Radioact. 137, 37–45. https://doi.org/10.1016/j.jenvrad.2014.06.017.
Thiry, Y., Garcia-Sanchez, L., Hurtevent, P., 2016. Experimental quantification of radiocesium recycling in a coniferous tree after aerial contamination: field loss dynamics, translocation and final partitioning. J. Environ. Radioact. 161, 42–50. https://doi.org/10.1016/j.jenvrad.2015.12.017.
Tsuruta, H., Oura, Y., Ebihara, M., Ohara, T., Nakajima, T., 2014. First retrieval of hourly atmospheric radionuclides just after the Fukushima accident by analyzing filter-tapes of operational air pollution monitoring stations. Sci. Rep. 4, 1–10. https://doi.org/10.1038/srep06717.
Tucker, A., Levia, F., Katul, G.G., Nanko, K., Rossi, L.F., 2020. A network model for stemflow solute transport. Appl. Math. Model. 88, 266–282. https://doi.org/10.1016/j.apm.2020.06.047.
Yoshihara, T., Matsumura, H., Tsuzaki, M., Wakamatsu, T., Kobayashi, T., Hashida, S. nosuke, Nagaoka, T., Goto, F., 2014. Changes in radiocesium contamination from Fukushima in foliar parts of 10 common tree species in Japan between 2011 and 2013. J. Environ. Radioact. 138, 220–226. https://doi.org/10.1016/j.jenvrad.2014.09.002.
Yoshihara, T., Matsumura, H., Hashida, S.nosuke, Nakaya, K., 2016. Radiocesium contamination in living and dead foliar parts of Japanese cedar during 2011-2015. J. Environ. Radioact. 164, 291–299. https://doi.org/10.1016/j.jenvrad.2016.08.010.
Zhiyanski, M., Sokolovska, M., Bech, J., Clouvas, A., Penev, I., Badulin, V., 2010. Cesium-137 contamination of oak (*Quercus petrae* Liebl.) from sub-mediterranean zone in South Bulgaria. J. Environ. Radioact. 101, 864–868. https://doi.org/10.1016/j.jenvrad.2010.05.011.